

Article

Modeling and Simulation of Hydroxyapatite Recovery in the Desliming Circuit of the Tapira Industrial Plant, Brazil

Adalto Silveira, Jr.^{1,2}, Homero Delboni, Jr.²  and Maurício Guimarães Bergerman^{2,*} ¹ Mosaic Fertilizantes P&K, Araxá 38184-270, Brazil² Department of Mining and Petroleum Engineering, Polytechnic School, University of São Paulo, São Paulo 05508-030, Brazil

* Correspondence: mbergerman@usp.br

Abstract: The modeling and simulation of industrial mineral processing operations are traditionally used for cyclone sizing and optimizations of industrial operations. However, the main models used are based on the total population of particles in the pulp, thus not distinguishing the individual minerals. This article presents the results of an innovative method that investigated the optimization of the metallurgical recovery of P₂O₅ in the desliming circuit of a phosphate ore processing plant in Brazil. A survey campaign was carried out in the existing industrial circuit, followed by determining the partition curves for the overall particles and specifically for the hydroxyapatite particles. The results were used to calibrate the Narasimha–Mainza cyclone model. From a Base Case determined with reference to the industrial survey, three optimization scenarios were simulated through cyclone geometries and respective operating conditions changes. Simulated scenarios indicated the possibility of P₂O₅ metallurgical recovery increasing from 9.4% to 12.7% compared to the Base Case.

Keywords: phosphate ore; desliming; simulation; modeling

Citation: Silveira, A., Jr.; Delboni, H., Jr.; Bergerman, M.G. Modeling and Simulation of Hydroxyapatite Recovery in the Desliming Circuit of the Tapira Industrial Plant, Brazil. *Minerals* **2024**, *14*, 272. <https://doi.org/10.3390/min14030272>

Academic Editors: Carlos Hoffmann Sampaio and Yutaro Takaya

Received: 13 December 2023
Revised: 19 February 2024
Accepted: 26 February 2024
Published: 4 March 2024



Copyright: © 2024 by the authors. Licensee MDPI, Basel, Switzerland. This article is an open access article distributed under the terms and conditions of the Creative Commons Attribution (CC BY) license (<https://creativecommons.org/licenses/by/4.0/>).

1. Introduction

Processing weathered apatitic phosphate ores includes separating the slimes' fraction to increase the selectivity in the downstream flotation concentration process [1–4]. Although beneficial to the concentration, this condition also results in significant losses of phosphorus-bearing minerals to the slimes. This combination results in the need to control each stage of an industrial desliming circuit to balance the benefits and losses of hydroxyapatite (HA) from the process. This last aspect is critical as slimes are diverted to tailings dams, which either reduces the life of these structures or increases the mass to be dewatered and piled up in high-cost operations, as recently occurring in Brazilian mining [5–7].

Cyclones are widely used in industrial classification operations mainly due to their versatility, high capacity and relative simplicity of operation. The forces acting on the particles determine downward trajectories for the relatively coarser ones and upward trajectories for the finer ones. The geometry of the cyclone, in combination with the operating conditions, modulates the partition of the solids in each particle size fraction. According to Delboni Jr. [8], the most widely used models for cyclone simulation were developed using hard ores, thus different from the relatively high amount of natural fines observed in most weathered Brazilian phosphate ores. Accordingly, the various mathematical models created in the last four decades [9–13] have been based on cyclones operating in comminution circuits, thus distinct from desliming circuits. Also, these models considered only one partition curve despite the individual minerals being classified.

Lynch and Rao [9] presented individual partition curves for the minerals limestone, silica and coal. Later in the same work, the authors showed the partition curve for the Warrego industrial operation and a theoretical partition curve based on the differences in specific weights of the minerals presented quartz and magnetite. In reference to the

Warrego ore partition curve, the authors considered that the tail was because the d50c values for the ore were not the weighted average for the d50c values for the components but were biased toward the lower value. Further calculations showed that the shape of the curve was affected by the size distributions of the components and their relative proportions. The conclusion was that a composite reduced efficiency curve may change, but the curves for the components remain constant.

More recently, the Narasimha–Mainza [14] semi-mechanistic mode was developed based on a comprehensive database considering different operating and design conditions, showing greater accuracy than previously widely used models. Accordingly, Equations (1)–(4) are used to predict the performance of the classification operation regarding, respectively, the recovery of water to the underflow (Rf), the corrected cut size (d50c), volumetric flow of slurry (Q) in the feed and sharpness of the separation (α). A fundamental point of the Narasimha–Mainza model is that although the density of solids is included in the equations, it refers to the bulk of particles, since the differences in performance for particles of different densities were not reported, or even validated.

$$Rf = Kw \left(\frac{Do}{Dc} \right)^{-1.06787} \left(\frac{Du}{Dc} \right)^{2.2062} \left(\frac{Vt^2}{Rmax \cdot g} \right)^{-0.20572} \left(\frac{1}{\tan\left(\frac{\theta}{2}\right)} \right)^{0.829} \left(\frac{\mu m}{\mu w} \right)^{-0.7118} \left(\frac{Lc}{Dc} \right)^{2.424} \left(\frac{Vh}{Vt} \right)^{-0.8843} \left(\frac{\rho s - \rho f}{\rho f} \right)^{0.523} \left(\cos\left(\frac{i}{2}\right) \right)^{1.793} \quad (1)$$

$$\left(\frac{d50c}{Dc} \right) = KD \left(\frac{Do}{Dc} \right)^{1.093} \left(\frac{Du}{Dc} \right)^{-1.00} \left(\frac{(1-fv)^2}{(10^{1.82fv})} \right)^{-0.703} (Re)^{-0.436} \left(\frac{Di}{Dc} \right)^{-0.936} \left(\frac{Lc}{Dc} \right)^{0.187} \left(\frac{1}{\tan(\theta)} \right)^{-0.1988} \left(\cos\left(\frac{i}{2}\right) \right)^{-1.034} \left(\frac{\rho s - \rho f}{\rho f} \right)^{-0.217} \quad (2)$$

$$Q = KQo \left(\frac{Di}{Dc} \right)^{0.45} Dc^2 \left(\frac{P}{\rho p} \right)^{\frac{1}{2}} \left(\frac{Do}{Dc} \right) \left(\frac{Du}{Dc} \right)^{0.037} \left(\frac{1}{\tan\left(\frac{\theta}{2}\right)} \right)^{0.405} \left(\frac{Lc}{Dc} \right)^{0.3} \left(\frac{Vh}{Vt} \right)^{-0.048} \left(\cos\left(\frac{i}{2}\right) \right)^{-0.092} \quad (3)$$

$$\alpha = \frac{K\alpha \left(\frac{Do}{Dc} \right)^{0.27} \left(\frac{Vt^2}{g \cdot Rmax} \right)^{0.016} \cos\left(\frac{i}{180}\right)^{0.868} \left(\frac{(1-fv)^2}{10^{1.82 \times fv}} \right)^{0.72}}{\left(\frac{Du}{Dc} \right)^{0.567} \left(\frac{\rho s - \rho p}{\rho s} \right)^{1.837} \left(\frac{\mu m}{\mu w} \right)^{0.127} \left(\frac{1}{\tan(\theta)} \right)^{0.182} \left(\frac{Lc}{Dc} \right)^{0.2}} \quad (4)$$

1.1. Objectivea

The main objective of this work was to investigate the optimization of the metallurgical recovery of P₂O₅ from the desliming stage of the phosphate ore beneficiation industrial circuit of Tapira-MG, Brazil, through a novel specific calibration and simulation of HA using the Narasimha–Mainza model.

1.2. Tapira Industrial Mineral Processing Plant

The Tapira phosphate ore processing plant, located in the state of Minas Gerais, Brazil, was implemented at the end of the 1970s and currently processes an average of 15.9 Mt per year, which results in a nominal feed flow rate of 1.950 t/h of solids. The annual production is 2 Mt of concentrate, thus ranking Tapira as the largest phosphate concentrator in Brazil. The plant feed grade of 8.5% P₂O₅ is upgraded to 35% P₂O₅ through initial multi-stage crushing steps, followed by a screening that splits the crushed feed into two different circuits. The hard ore circuit processes the coarse fraction, i.e., −19.1 + 7.0 mm, while the soft ore circuit is fed with the −7.0 mm fraction, representing nearly 80% of overall plant feed.

The soft ore circuit feed slurry is pumped and split into four parallel lines, each one including an initial classification stage carried out in a nest of 508 mm diameter cyclones, followed by processing the cyclone's coarse fraction in a dedicated grinding circuit, which

also includes magnetite separation in magnetic drums, as shown in the flow sheet of Figure 1.

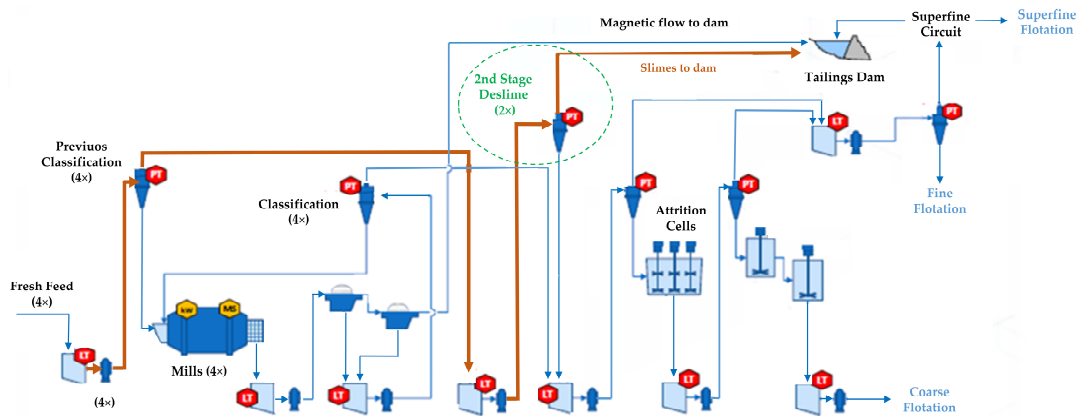


Figure 1. Tapira industrial plant flowsheet—soft ore circuit.

Figure 1 also shows that the joined overflow from the initial classification stage, referred to as natural fines, is further classified in two parallel lines, each consisting of 16 cyclones of 254 mm in diameter, called the second desliming stage. The latter is the focus of the present work.

The combined second desliming stage underflow is pumped to another classification stage, resulting in coarse and fine flotation feed circuits. In contrast, the combined second desliming stage overflow is transferred to the tailing dam.

The optimal operation of the second desliming stage consists of efficiently separating the slimes with the maximum possible recovery of HA to the combined underflow. While the former is essential for a high flotation performance, the latter modulates the P_2O_5 recovery in the industrial circuit. Based on the overall plant feed, the mass split to the two parallel second desliming stages is rated at 15%. Due to practical and operational aspects, the present study focused exclusively on one of the two secondary desliming lines. As the equipment and operating conditions are identical, the results were considered replicable for either of the two lines.

2. Materials and Methods

2.1. Method

A comprehensive survey was carried out at the second desliming stage at the Tapira industrial plant. It included sampling feed, underflow and overflow of one nest of cyclones, obtaining detailed data and information from the dedicated process information management system (PIMS), and measuring vortex and apex from selected equipment. The collected samples were processed in the Tapira Process Laboratory Unit (LPUT) to determine respective solids concentration, size distribution and chemical analysis of size-by-size products. Further sample characterization was conducted at the Mineral Processing Laboratory of the Polytechnic School of the University of São Paulo (LTM-EPUSP) for assessing the size distribution of fines by Cyclosizer, as well as X-ray Diffraction (XRD) analysis at the Technological Ore Characterization Laboratory of the Polytechnic School of the University of São Paulo (LCT-EPUSP). Mass balancing experimental data and mathematical model calibration were carried out using Excel 365 and JKSimMet 6.2 software. The flowsheet described in Figure 2 shows the sequence described above.

2.2. Survey Campaign

The industrial sampling campaign was carried out during a steady-state operation of the Tapira processing plant. Sampling points of the second desliming stage are listed in Table 1. During the stabilization and sampling periods, 13 cyclones were in full operation.

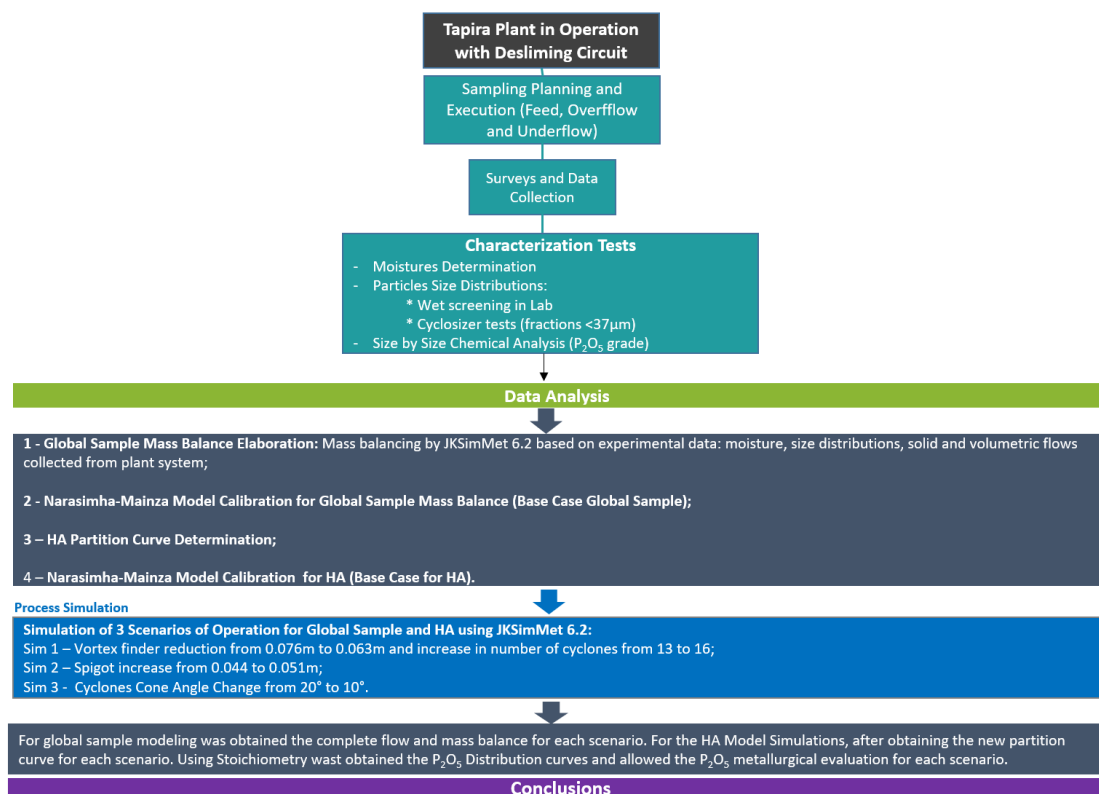


Figure 2. Method adopted in the present work.

Table 1. Sampling points.

Sampling Point	Description
1	Second desliming feed
2	Second desliming underflow
3	Second desliming overflow

Sampling points 2 and 3 in Table 1 consisted of combined flows, respectively, of the underflow and overflow of the 13 cyclones in operation. Sampling was carried out incrementally every 10 min for two hours to obtain sufficient mass for the sample processing for the three flows sampled. Circuit stabilization was assessed by three main indicators listed in the PIMS the plant fresh feed rate, cyclone nest feed pressure and pulp flow rate, and feed sump level. The cyclone nest feed flow rate of solids was calculated based on the pulp flow rate, as indicated by the PIMS, and the concentration of the solids obtained from the cyclone feed sample. Figure 3 shows a photograph of the secondary desliming stage installed at the Tapira industrial plant.

2.3. Sample Processing

The collected samples were initially weighed, filtered and then dried in an oven at the LPUT to determine the concentration of solids by weight (Cw).

Dry samples were split and screened at the following laboratory sieves: 0.500; 0.230; 0.152; 0.106; 0.074; 0.053; 0.044; and 0.037 mm. In each case, triplicate screening was carried out to obtain sufficient chemical analysis mass. Except for the fraction passing at 0.037 mm sieve, all other fractions were oven-dried, weighted and prepared for chemical analysis at the Mosaic laboratories.

Fractions passing at 0.037 mm were tested at a Cyclosizer installed at the LTM-EPUSP. Due to mass constrain as stipulated in Cyclosizer standard procedure, each sample from each stream, i.e., cyclone feed, underflow and overflow, was divided into six sub-samples

for testing at the Cyclosizer, therefore totaling 18 Cyclosizer tests. Based on the results, only 0.025 mm (products of C1, C2 and C3 from the Cyclosizer) and 0.013 mm (products of C4 and C5 from the Cyclosizer) were adopted for reporting the Cyclosizer results. The obtained $-0.037 + 0.025$ mm, $-0.025 + 0.013$ mm and -0.013 mm fractions of cyclone feed, underflow and overflow were returned to the Tapira for chemical analysis.



Figure 3. Tapira industrial circuit—second desliming stage.

The cyclone feed sample was further prepared for semi-quantitative mineralogical analysis via X-ray Diffraction (XRD) at LCT-EPUSP.

2.4. Mass Balance and Calibration of the Narasimha–Mainza Model

The mass balance of experimental data was carried out based on the concentration of solids and size distributions of the cyclone feed, underflow and overflow, as well as on the cyclone feed solids' flow rate. Data from mass balance were further used to calibrate the Narasimha–Mainza model, thus resulting in the calibrated model, here referred to as Base Case.

2.5. Determination of the Partition Curve and Cyclone Model Calibration for HA

In addition to calibrating the Narasimha–Mainza model for overall cyclone feed, underflow and overflow, the same model was calibrated specifically for the mineral HA, following the adopted procedures described in Sections 2.5.1–2.5.3.

2.5.1. Determination of HA Distributions

The calculation of HA content in each size fraction of each stream around the cyclone was based on the XRD analysis results shown in Appendix A, which indicated that the only phosphorus-bearing mineral in the ore is HA.

The conversion of P_2O_5 grades obtained from chemical analysis to HA grades was stoichiometric, i.e., by calculating the grade of P_2O_5 in the HA formula. The result indicated a factor of 2.36.

Equation (5) was used to calculate the experimental distributions of apatite in each particle size fraction for the feed, overflow and underflow.

$$CAP_i = \frac{x_i \cdot a_i \cdot cf}{\sum_{k=0}^i (x_k \cdot a_k \cdot cf)} \quad (5)$$

where:

CAP_i = HA content in size fraction i ;
 x_i = percent retained in size fraction i ;
 a_i = P_2O_5 grade in size fraction i ;
 i = number of size fractions;
 cf = conversion factor of P_2O_5 to HA (2.36).

The results obtained from Equation (5) were balanced for consistency in the HA distributions in the cyclone feed, underflow and overflow. The consistency criterion adopted using a simple two-product formula to calculate the overall mass partition (R_m) around the cyclone streams.

2.5.2. Parameterization of HA Partition Curve

The partition of apatite by particle size fraction (U_i) was calculated.

The obtained corrected partition distribution curve was parameterized by Whiten's formula, shown in Equation (6).

$$U_i = \frac{e^{\alpha y_i} - 1}{e^{\alpha y_i} + e^{\alpha y_i} - 2} \quad (6)$$

The parameter y_i represents the ratio between particle size and d_{50c} , the latter corresponding to the size associated with a 50% corrected partition. In the same Equation (6), the α parameter represents the dispersion of the corrected partition distribution around d_{50c} .

2.5.3. Model Calibration

The parameters d_{50c} and α , obtained from the parameterization of the HA partition curve, were used to calibrate the respective model equations in Narasimha–Mainza, i.e., Equations (2) and (4). The calibration of Equation (2), relative to parameter d_{50c} , consisted of calculating the constant KD , while the calibration of Equation (4), relative to parameter α consisted of calculating the constant $K\alpha$.

2.6. Simulations

The simulations were carried out in two steps. In the first, the calibrated Narasimha–Mainza model was used to simulate overall mass and water flow rates around cyclone feed, underflow and overflow. The second simulation obtained the HA partitions based on specifically calibrated Equations (2) and (4), also based on the Narasimha–Mainza model. Accordingly, the obtained size distributions and HA distributions of underflow and overflow were used to calculate the P_2O_5 grade in each size fraction of these two streams. The feed size distribution and HA distributions were kept constant for the cyclone feed stream.

Three complete simulations were conducted to increase the overall HA recovery to the deslimed flow (cyclone underflow), together with relatively small variations in the amount of fines in the same stream.

3. Results and Discussion

This section describes the results obtained from the industrial survey, sample characterization, mass balance and model calibration results. The simulation obtained for the second desliming stage results of the Tapira industrial plant is also presented and discussed.

3.1. Industrial Sampling Results

The main characteristics of the cyclones and the selected operating variables obtained during the survey campaign, are listed in Table 2.

Table 2. Cyclone geometry and operating conditions.

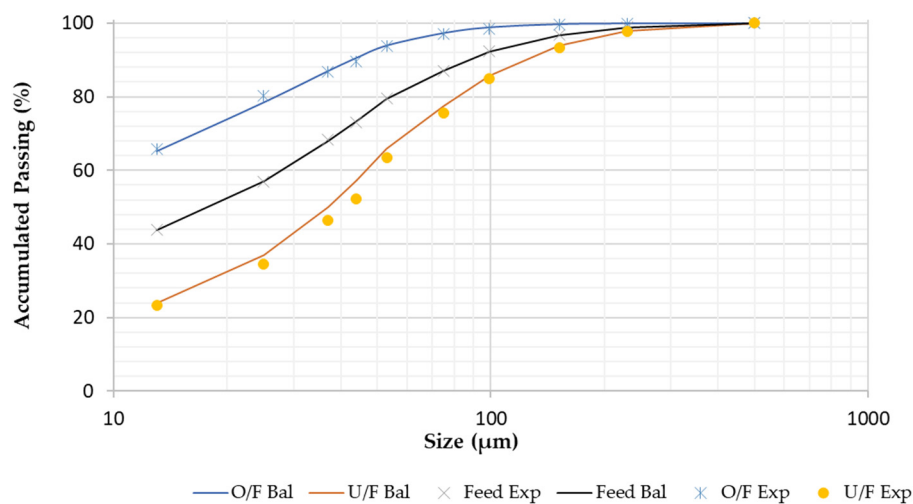
Cyclone Geometry and Operating Conditions	
Solids Feed Rate (2nd Desliming Feed) (t/h)	256
Feed Concentration of Solids (%)	14.0
Operational Pressure (kgf/cm ²)	2.70
Cyclone Diameter—Dc (m)	0.254
Inlet Diameter—Di (m)	0.063
Vortex Finder Diameter—Do (m)	0.076
Spigot Diameter—Du (m)	0.044
Cylinder Length—Lc (m)	0.200
Cone Angle—Theta (°)	20
Inclination Angle (°)	0
Units in Parallel	13

3.2. Mass Balance and Model Calibration

This section presents the mass balance results and the calibration of the Narasimha–Mainza model.

3.2.1. Experimental and Mass Balance Data

Figure 4 shows experimental and mass balanced particle size distributions. Table A1 in Appendix B illustrates all the detailed data from the sampling. It can be seen that the experimental and balanced results are very close, illustrating the quality of the sampling.

**Figure 4.** Size distributions of the cyclone feed, underflow and overflow.

3.2.2. Model Calibration for Overall Flows

The selected parameters for model calibration, as obtained from mass balance calculations, are listed in Table 3.

Table 3. Cyclone operation selected parameters.

Cyclone Operation Selected Parameters	
Water Split To O/F (%)	79.4
Corrected d50 (mm)	0.029
Operating Pressure (kPa)	264
Sharpness of Efficiency Curve— α	0.302

The calibration constants obtained for the Narasimha–Mainza from Equations (1)–(4) based on mass-balanced overall flows are listed in Table 4.

Table 4. Calibration constants for the Narasimha–Mainza model.

Model Parameters	
d50c Constant—K _{D0}	0.030
Capacity Constant—K _{Q0}	635
Water Split Constant—K _{W1}	13.55
Sharpness Constant—K _α	0.562

The corrected partition curve obtained from model calibration is shown in Figure 5.

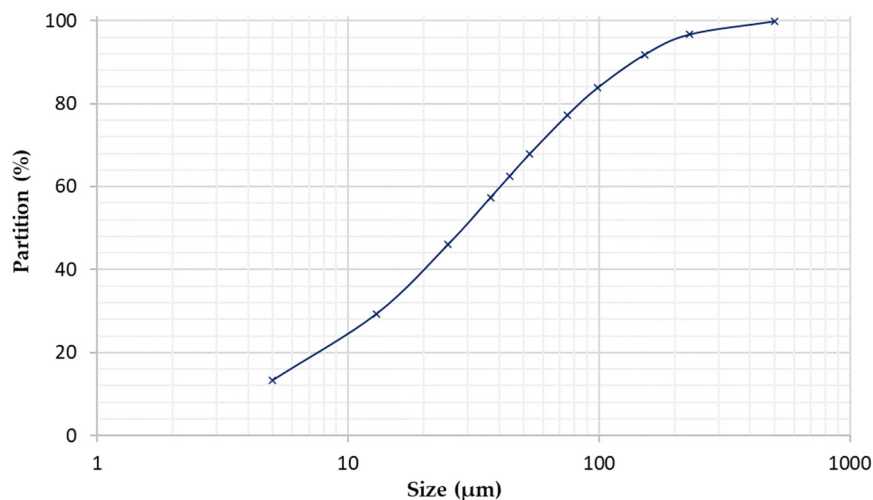


Figure 5. Corrected partition curve for overall flows around the cyclone nest.

3.3. HA Balancing and Partition Modelling

The results obtained from the HA partition curve parameterization and model calibration are presented in the following sections.

3.3.1. HA Distribution

Table 5 presents the experimental and balanced HA distributions for each of the three cyclone flows. Table A2 in Appendix B shows for each stream around the cyclones, the balanced particle size, together with experimental P₂O₅ grades and the resulted experimental HA distribution.

Table 5. Balanced HA distributions.

Size (mm)	Experimental HA Distribution			Balanced HA Distribution		
	Feed	Overflow	Underflow	Feed	Overflow	Underflow
0.500	100	100	100	100	100	100
0.230	99.40	99.99	99.21	99.40	100.00	99.08
0.152	98.29	99.93	97.38	98.29	100.00	97.39
0.099	94.55	99.61	91.84	94.52	99.97	91.65
0.075	88.54	98.58	82.58	88.56	99.64	82.72
0.053	76.21	95.63	66.49	76.47	96.96	65.68
0.044	67.25	92.30	54.59	67.97	93.02	54.79
0.037	59.33	88.36	44.31	58.36	86.51	43.55
0.025	35.20	62.78	20.87	35.73	63.27	21.22
0.013	20.96	42.87	9.03	20.95	41.78	9.99

Figure 6 shows the cyclone nest feed, overflow, and underflow distributions' balanced HA distributions.

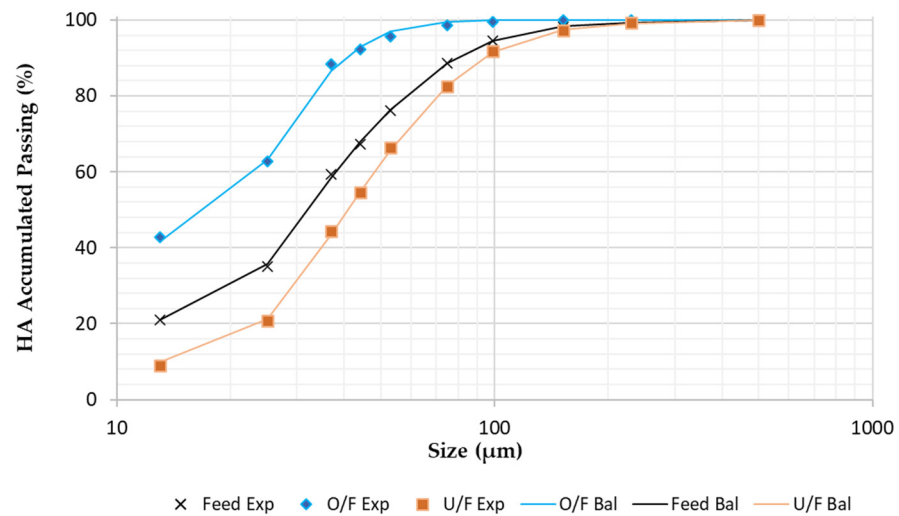


Figure 6. HA experimental and balanced data.

3.3.2. Model Calibration for HA Partition

The balanced HA distributions were used to calculate the respective HA partitions, parameterized in terms of d_{50c} and α , as shown in Table 6. Based on these two parameters, the constants K_D and $K\alpha$, for Equations (2) and (4) of the Narasimha–Mainza model were calculated. The obtained values are shown in Table 7.

Table 6. Selected parameters for the HA partition curve.

Selected HA Partition Curve Parameters	
Corrected d_{50c} (mm)	0.030
Sharpness of Efficiency Curve— α	1.75

Table 7. HA partition curve calibration constants.

HA Model Parameters	
d_{50c} Constant— K_D	0.032
Sharpness Constant— $K\alpha$	3.235

The obtained HA partition curve is shown in Figure 7.

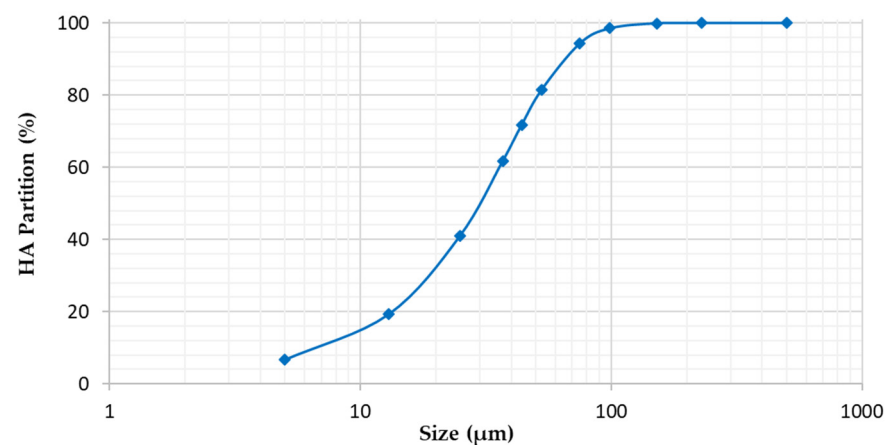


Figure 7. HA partition curve.

The first calibration exercise for the global sample indicated relatively small sharpness of the overall partition curve ($\alpha = 0.302$), which may be misinterpreted as a low performance of the classification process. The second step, though, revealed a relatively high performance of the classification process specifically for the HA ($\alpha = 1.75$). Thus, such a result is paramount, as an apparently low-performance classification is a high-performance one. This aspect was already masterfully assessed in the seminal work by Lynch and Rao [9].

3.4. Simulations

The simulations aimed at increasing the recovery of HA in the deslimed flow (cyclone underflow) while resulting in relatively small variations in the amount of fines in the same stream as compared with the Base Case. Simulated conditions included changes in the geometry of the cyclones, i.e., apex and vortex diameters, conical section inclination and changing the number of units in operation for adjusting the operating pressure. Table 8 shows the simulated changes as compared to the Base Case.

Table 8. Simulated scenarios.

Geometry Aspects and Operating Conditions				
	Base Case	Sim 1	Sim 2	Sim 3
Cyclone Diameter—Dc (m)	0.254	0.254	0.254	0.254
Inlet Diameter—Di (m)	0.063	0.063	0.063	0.063
Vortex Finder Diameter—Do (m)	0.076	0.063	0.076	0.076
Spigot Diameter—Du (m)	0.044	0.044	0.051	0.044
Cylinder Length—Lc (m)	0.200	0.200	0.200	0.200
Cone Angle—Theta (°)	20	20	20	10
Inclination Angle (°)	0	0	0	0
Units in Parallel	13	16	13	13
Operational Pressure (KPa)	264	278	259	149

3.4.1. Simulation Results—Cyclones' Overall Operation

The results obtained from the three simulations are presented in Table 9, together with the Base Case.

Compared with the Base Case, the three simulations significantly increased the flow rate of solids in the cyclone underflow. Accordingly, simulation 1 resulted in 146 t/h compared to 132 t/h of solids in the Base Case, an increase of 10.6%. Similarly, simulations 2 and 3 resulted in underflow solids flow rate increases of 12.9% and 16.7%, respectively. The same simulations also indicated moderate fines increases in the underflow, in this case, the fraction finer than 0.013 mm.

3.4.2. HA Simulations

The same conditions selected for the three simulations were used to simulate the HA distributions to cyclone' underflow and overflow in each case. Table 10 presents the results obtained for the HA distributions and the Base Case.

Table 10 indicates significantly higher HA partitions for the underflow relative to the Base Case. Considering the 66% HA partition figure as a reference in the Base Case, the three simulations resulted in HA partitions in the range of 72%–74%. The relative HA increases to underflow were 9.4%, 11.1% and 12.7%, respectively, for simulations 1, 2 and 3.

Table 11 shows the HA partition curve parameters for the Base Case and those calculated for the other three simulations. The respective HA partition curves were plotted based on these parameters, as shown in Figure 8.

Table 9. Simulation results—overall streams.

	Base Case			Simulation 1			Simulation 2			Simulation 3		
	Feed	Overflow	Underflow	Feed	Overflow	Underflow	Feed	Overflow	Underflow	Feed	Overflow	Underflow
Solids Flowrate (t/h)	256	124	132	256	110	146	256	107	149	256	102	154
Mass Partition (%)	100	48	52	100	43	57	100	42	58	100	40	60
Solids SG (t/m ³)	2.70	2.70	2.70	2.70	2.70	2.70	2.70	2.70	2.70	2.70	2.70	2.70
Water Flowrate (t/h)	1573	1249	324	1573	1151	422	1573	1125	447	1573	1062	510
% Solids	14.0	9.0	28.9	14.0	8.7	25.8	14.0	8.7	25.0	14.0	8.8	23.2
Pulp SG (t/m ³)	1.10	1.06	1.22	1.10	1.06	1.19	1.10	1.06	1.19	1.10	1.06	1.17
Volumetric Flowrate (m ³ /h)	1667	1295	373	1667	1192	476	1667	1165	503	1667	1100	567
Size (mm)												
0.500	0	0	0	0	0	0	0	0	0	0	0	0
0.230	1.14	0.04	2.18	1.14	1.14	1.97	1.14	0.03	1.94	1.14	0.03	1.88
0.152	2.14	0.19	3.97	2.14	2.13	3.61	2.14	0.16	3.55	2.14	0.15	3.44
0.099	4.55	0.88	8.02	4.55	4.64	7.54	4.55	0.78	7.41	4.55	0.79	7.20
0.075	4.96	1.53	8.16	4.96	4.79	7.37	4.96	1.33	7.26	4.96	1.34	7.06
0.053	7.74	3.40	11.84	7.74	7.92	11.46	7.74	3.20	11.31	7.74	3.25	11.02
0.044	6.04	3.38	8.54	6.04	5.92	8.02	6.04	3.10	7.94	6.04	3.14	7.76
0.037	5.49	3.58	7.27	5.49	5.58	7.17	5.49	3.43	7.11	5.49	3.49	6.96
0.025	10.90	8.55	13.12	10.90	10.82	12.80	10.90	8.14	12.74	10.90	8.24	12.52
0.013	13.22	13.35	13.10	13.22	13.25	13.24	13.22	13.24	13.26	13.22	13.35	13.19
−0.013	43.82	65.10	23.80	43.82	43.82	26.82	43.82	66.59	27.48	43.82	66.22	28.97

Table 10. Simulation results—HA distributions.

	Base Case			Simulation 1			Simulation 2			Simulation 3		
	Feed	Overflow	Underflow									
Apatite Partition (%)	100	34	66	100	28	72	100	27	73	100	26	74
Size (mm)												
	Retained (%)			Retained (%)			Retained (%)			Retained (%)		
0.500	0	0	0	0	0	0	0	0	0	0	0	0
0.230	0.60	0.00	0.92	0.60	0.00	0.83	0.60	0.00	0.82	0.60	0.00	0.80
0.152	1.11	0.00	1.69	1.11	0.00	1.54	1.11	0.00	1.52	1.11	0.00	1.48
0.099	3.78	0.03	5.75	3.78	0.02	5.24	3.78	0.02	5.16	3.78	0.02	5.05
0.075	5.96	0.33	8.92	5.96	0.21	8.20	5.96	0.22	8.08	5.96	0.20	7.91
0.053	12.09	2.68	17.04	12.09	2.01	16.01	12.09	2.03	15.79	12.09	1.97	15.50
0.044	8.49	3.94	10.89	8.49	3.25	10.54	8.49	3.25	10.43	8.49	3.25	10.27
0.037	9.61	6.50	11.24	9.61	5.68	11.14	9.61	5.66	11.07	9.61	5.73	10.92
0.025	22.63	23.24	22.33	22.63	21.95	22.91	22.63	21.80	22.95	22.63	22.22	22.78
0.013	14.78	21.49	11.23	14.78	21.75	12.05	14.78	21.67	12.23	14.78	21.91	12.36
−0.013	20.96	41.78	9.99	20.96	45.12	11.52	20.96	45.35	11.96	20.96	44.69	12.93

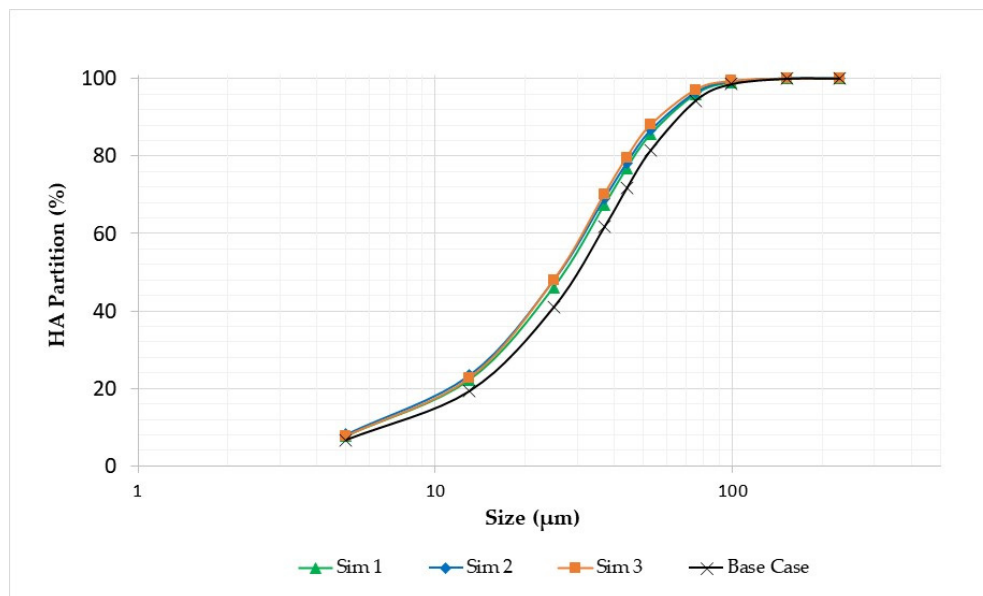


Figure 8. Base Case and simulated HA partition curves.

Table 11 shows no significant differences among the d_{50c} and α parameters of the HA partition curves calculated for the Base Case and the three additional simulations. However, the Graph in Figure 8 shows significant partition increases of HA in fractions of intermediate size, particularly in the $-0.075 + 0.013$ mm range. Conversely, simulated HA partitions for fractions coarser than 0.075 mm and finer than 0.013 mm virtually coincided with the Base Case. The combination of the simulated significant increase in HA in the $-0.075 + 0.013$ mm range and the high HA content in the same size range in the cyclone feed resulted in the simulated HA increase in the 9.4%–12.7% range.

3.4.3. Comparisons between Mass and HA Recoveries

Table 12 shows the absolute and relative global mass and P_2O_5 recoveries to the cyclone underflow for the Base Case and all three simulations.

Table 11. d_{50c} e alfa parameters for the HA Base Case and simulations.

Selected HA Partition Curve Parameters			
Scenario	d_{50c} (µm)	α	Partition to Underflow (%)
Base Case	30	1.75	65.9
Simulation 1	27	1.68	71.7
Simulation 2	26	1.63	72.9
Simulation 3	27	1.77	74.4

Table 12. Summary of overall mass and P_2O_5 recovery for the simulated scenarios.

Index	Base Case	Simulation		
		1	2	3
Mass Recovery to Underflow (%)	51.5	57.1	58.2	60.2
Relative variation to Base Case (%)	-	10.9	13.1	16.8
P_2O_5 Metallurgical Recovery to Underflow (%)	65.7	71.8	73.0	74.0
Relative variation to Base Case (%)	-	9.4	11.1	12.7

Table 12 shows more significant mass recoveries than P_2O_5 recoveries for all three simulations, thus indicating that the conventional approach of estimating cyclone perfor-

mance based solely on mass recovery is not necessarily adequate for assessing metallurgical recovery. The HA simulated partitions based on calibrated equations to estimate partition curve parameters provided a suitable method for predicting the distribution of HA in each size fraction, as well as on the overall streams of the cyclone.

Further detailed simulations could have explored the reduction in the total fines of the cyclone underflow stream compared with the Base Case. Such exercises were not carried out as a comprehensive approach would include assessing the downstream flotation process, which was out of the scope of the present work.

4. Conclusions and Recommendations

The present work investigated an innovative method to estimate the metallurgical performance of an industrial desliming process through the parameterization of a selected mineral partition, therefore differing from the traditional approach based solely on overall mass flows. The method was applied to the Tapira industrial phosphate plant, where the operation of the selected desliming stage aims to reduce the amount of fines in the flotation downstream process. Reducing the Hydroxyapatite (HA) losses to the cyclone overflow (slimes) is critical to increasing the metallurgical recovery of such a mineral in the overall beneficiation process.

The method described here is based on a two-step calibration of the Narasimha–Mainza cyclone model. The first includes overall flow rates around the cyclone, whereas the second consists of calibrating the Narasimha–Mainza equations for the partition curve for the selected mineral. The first calibration exercise indicated a relatively small sharpness of the overall partition curve ($\alpha = 0.302$), which may be misinterpreted as a low performance of the classification process. The second step, though, reveals a relatively high performance of the classification process specifically for the HA ($\alpha = 1.75$). Thus, such a result is paramount, as an apparently low-performance classification is a high-performance one.

Simulations with the calibrated model indicated significant improvements in the HA metallurgical recovery, ranging from 9.4% to 12.7%, through relatively simple changes in the vortex or apex apertures, as well as adjusting the operating feed pressure by variation in the number of cyclones in operation.

The proposed method also has potential applications in industrial grinding circuits, where differences in density and/or shape of minerals result in different partitions in cyclones operating in closed configurations with ball mills. In such cases, the classification performance of the selected mineral may be improved, avoiding overgrinding.

Author Contributions: Conceptualization, A.S.J. and H.D.J.; methodology and validation, A.S.J., M.G.B. and H.D.J.; formal analysis, A.S.J., M.G.B. and H.D.J.; writing—original draft preparation, A.S.J.; writing—review and editing, M.G.B. and H.D.J.; supervision, H.D.J. All authors have read and agreed to the published version of the manuscript.

Funding: This research received no external funding.

Data Availability Statement: Data are contained within the article.

Acknowledgments: Special thanks to Mosaic Fertilizantes for allowing and strongly supporting the development of this study. The encouragement, pioneering vision and research support culture of Mosaic Fertilizantes contributed to the realization of this work. Thanks to the LTM-EPUSP and LCT-EPUSP for their support during the characterization tests.

Conflicts of Interest: Adalto Silveira Júnior is the employee of Mosaic Fertilizantes P&K. The authors declare no conflicts of interest.

Nomenclature

D_c	cyclone diameter (m)
D_o	vortex finder diameter (m)
D_u	spigot diameter (m)
D_i	inlet equivalent diameter (m)
L_c	cylinder length (m)
θ	cone angle of cyclone (degree)
P	cyclone inlet pressure (kPa)
ρ	density (t/m^3) p = pulp, s = solids. f = fluid (t/m^3)
g	acceleration due to gravity ($9.81 m/s^2$)
Q_f	feed volume flow rate (m^3/h)
R_f	fraction of feed water to underflow
R_v	volumetric recovery of feed to underflow
R_{max}	cyclone cylinder section radius (m)
C_v	feed volume percent solids
fv	feed volume fraction of solids
i	inclination angle (degree)
Re	Reynolds number
V_h	particle hindered settling velocity (m/s)
V_t	particle terminal settling velocity (m/s)
μ	fluid viscosity (m,p = pulp, w,l = water)
λ	ratio between particle terminal settling velocity and particle hindered settling velocity, calculated as a function of feed volume percent solids:

$$\lambda = \frac{10^{1.82C_v}}{8.05(1-C_v)^2}$$

Appendix A

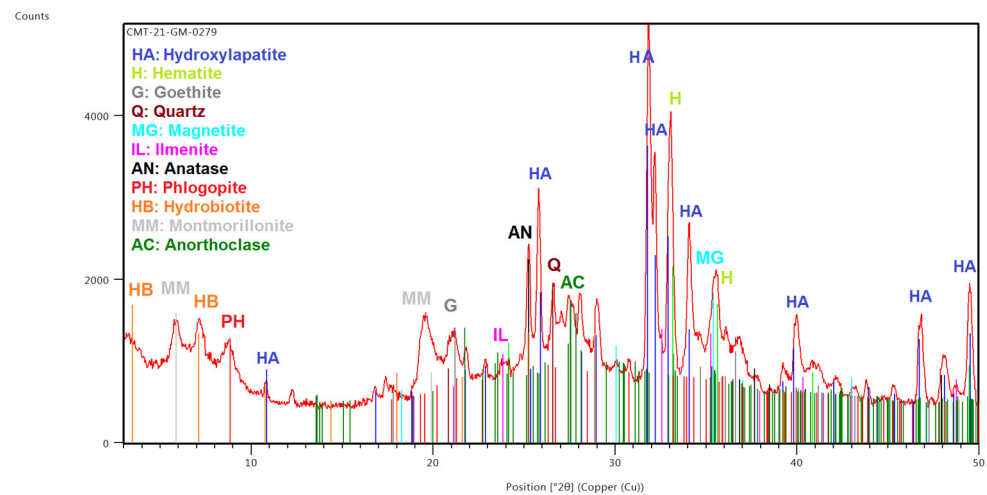


Figure A1. XRD results obtained from second desliming stage feed sample.

Appendix B

Table A1. Experimental and mass balanced data.

	Experimental Data			Mass Balance		
	Feed	Overflow	Underflow	Feed	Overflow	Underflow
Solids Flowrate (t/h)	256.0	-	-	256.0	124.1	131.9
Water Flowrate (t/h)	-	-	-	1572.6	1248.9	323.7
% Solids	14.0	10.1	25.9	14.0	9.0	28.9
Pulp SG (t/m ³)	-	-	-	1.10	1.06	1.22
Volumetric Flowrate (m ³ /h)	1667	-	-	1667	1295	373
Size (mm)	Size Distribution (Retained %)			Size Distribution (Retained %)		
0.500	0	0	0	0	0	0
0.230	1.14	0.11	2.36	1.14	0.04	2.18
0.152	2.16	0.37	4.32	2.14	0.19	3.97
0.099	4.37	0.98	8.50	4.55	0.88	8.02
0.075	5.29	1.59	9.13	4.96	1.53	8.16
0.053	7.51	3.24	12.25	7.74	3.40	11.84
0.044	6.40	4.19	11.22	6.04	3.38	8.54
0.037	4.77	2.76	5.85	5.49	3.58	7.27
0.025	11.53	6.49	11.90	10.90	8.55	13.12
0.013	13.01	14.47	11.12	13.22	13.35	13.10
-0.013	43.82	65.80	23.35	43.82	65.10	23.80

Table A2. Mass balanced size distributions, experimental P₂O₅ grades and HA experimental distributions.

Size (mm)	Feed			Overflow			Underflow		
	Mass Balanced Size Distribution Retained %	Experimental P ₂ O ₅ Grade (%)	Experimental HA Distribution (%)	Mass Balanced Size Distribution Retained %	Experimental P ₂ O ₅ Grade (%)	Experimental HA Distribution (%)	Mass Balanced Size Distribution Retained %	Experimental P ₂ O ₅ Grade (%)	Experimental HA Distribution (%)
0.500	0	0	0	0	0	0	0	0	0
0.230	1.14	2.97	0.60	0.04	1.28	0.01	2.18	2.72	0.79
0.152	2.14	2.94	1.11	0.19	1.13	0.05	3.97	3.45	1.83
0.099	4.55	4.64	3.74	0.88	1.48	0.33	8.02	5.16	5.53
0.075	4.96	6.83	6.00	1.53	2.65	1.03	8.16	8.49	9.26
0.053	7.74	9.00	12.34	3.41	3.43	2.95	11.84	10.17	16.09
0.044	6.04	8.37	8.95	3.38	3.91	3.33	8.54	10.43	11.90
0.037	5.49	8.14	7.92	3.58	4.35	3.93	7.27	10.58	10.28
0.025	10.90	12.50	24.14	8.55	11.86	25.58	13.12	13.37	23.44
0.013	13.22	6.08	14.24	13.35	5.91	19.91	13.10	6.76	11.84
-0.013	43.82	2.70	20.96	65.10	2.61	42.87	23.80	2.84	9.03
Total	100	5.65	100	100	3.96	100	100	7.48	100

References

- Yu, Y.; Ma, L.; Cao, M.; Liu, Q. Slime Coatings in Froth Flotation: A Review. *Miner. Eng.* **2017**, *114*, 26–36. [CrossRef]
- Abouzeid, A.Z.M. Physical and Thermal Treatment of Phosphate Ores—An Overview. *Int. J. Miner. Process.* **2008**, *85*, 59–84. [CrossRef]
- Derhy, M.; Taha, Y.; Hakkou, R.; Benzaazoua, M. Review of the Main Factors Affecting the Flotation of Phosphate Ores. *Minerals* **2020**, *10*, 1109. [CrossRef]
- Sis, H.; Chander, S. Reagents Used in the Flotation of Phosphate Ores: A Critical Review. *Miner. Eng.* **2003**, *16*, 577–585. [CrossRef]
- Silva, A.C.; Silva, E.M.S.; Da Silva Junior, Â.P.; Arruda, J.P.A.; De Araújo Vaz, V.R. Produção de Pasta a Partir de Rejeitos de Rochas Fosfáticas. *Rev. Esc. Minas* **2015**, *68*, 103–108. [CrossRef]
- Moukannaa, S.; Loutou, M.; Benzaazoua, M.; Vitola, L.; Alami, J.; Hakkou, R. Recycling of Phosphate Mine Tailings for the Production of Geopolymers. *J. Clean. Prod.* **2018**, *185*, 891–903. [CrossRef]
- Gomes, R.B.; De Tomi, G.; Assis, P.S. Iron Ore Tailings Dry Stacking in Pau Branco Mine, Brazil. *J. Mater. Res. Technol.* **2016**, *5*, 339–344. [CrossRef]
- Delboni Júnior, H. Modelling of Large Cone Angle Hydrocyclones. In *Proceedings of the Applied Research in the Minerals Industry*; Julius Kruttschnitt Mineral Research Centre: Indooroopilly, Australia, 1994.
- Lynch, A.J.; Rao, T.C. Modeling and Scale up of Hydrocyclone Classifiers. In *Proceedings of the International Mineral Processing Congress*, Cagliari, Italy, 20–26 April 1975.
- Plitt, L.R. A Mathematical Model of The Hydrocyclone Classifier. In *Proceedings of the CIM Bulletin*; Canadian Institute of Mining, Metallurgy and Petroleum: Wstmount, QC, Canada, 1978.

11. Nageswararao, K. Further Modelling and Scale Up of Hydrocyclones. Ph.D. Thesis, University of Queensland, Brisbane, Australia, 1978.
12. Svarovsky, L. *Hydrocyclones*; Rinehart and Winson: New York, NY, USA, 1984.
13. Tavares, L.M.; Souza, L.L.G.; Lima, J.R.B.; Possa, M.V. Modeling Classification in Small-Diameter Hydrocyclones under Variable Rheological Conditions. *Miner. Eng.* **2002**, *15*, 613–622. [[CrossRef](#)]
14. Narasimha, M.; Mainza, A.N.; Holtham, P.N.; Powell, M.S.; Brennan, M.S. A Semi-Mechanistic Model of Hydrocyclones—Developed from Industrial Data and Inputs from CFD. *Int. J. Miner. Process.* **2014**, *133*, 1–12. [[CrossRef](#)]

Disclaimer/Publisher’s Note: The statements, opinions and data contained in all publications are solely those of the individual author(s) and contributor(s) and not of MDPI and/or the editor(s). MDPI and/or the editor(s) disclaim responsibility for any injury to people or property resulting from any ideas, methods, instructions or products referred to in the content.